CrystEngComm

ROYAL SOCIETY OF CHEMISTRY

PAPER

View Article Online
View Journal | View Issue

Cite this: *CrystEngComm*, 2022, **24**, 1924

Synthesis, structure and properties of coordination polymers formed from bridging 4-hydroxybenzoic acid anions†

Brendan F. Abrahams, *[a] Christopher J. Commons, [a] A. David Dharma,[a] Timothy A. Hudson,[a] Richard Robson,[a] Robin W. Sanchez Arlt, [a] Thomas C. Stewart[b] and Keith F. White[ab]

Received 3rd February 2022,
Accepted 14th February 2022

DOI: 10.1039/d2ce00163b

rsc.li/crystengcomm

The combination of 4-hydroxybenzoic acid (H_2hba) with Li^+, Mg^{2+} and Cu^{2+} yields coordination polymers in which metal centres are bridged by an anion of the acid, either $Hhba^-$ or hba^{2-}. In the case of Li^+, a 3D network of composition Li_2(hba)DMF was isolated in which parallel channels are occupied by coordinated DMF molecules. Mg^{2+} combines with H_2hba to form a 2D square grid network with the formula $Mg(Hhba)_2(H_2O)_2$. The alignment of parallel sheets results in the formation of channels filled with 1,4-dioxane molecules that hydrogen bond to coordinated water molecules. The compound $Cu_3(hba)_2(OH)_2(1,4\text{-dioxane})_{1.5}\cdot 0.5(1,4\text{-dioxane})$ is a complex 3D network formed from the combination of Cu^{2+} with H_2hba under basic conditions. The crystal structure determination reveals bridging 1,4-dioxane molecules. A reversible phase change occurs in the temperature range 200–220 K. The investigation highlights the key role of the solvent molecules in the structures of this series of compounds.

Introduction

Coordination networks with largely ionic interactions between metal centres and bridging anions have been the focus of considerable attention over the last 12 years.[1–3] In regard to such materials, our group has had a long-standing interest in the generation of porous lightweight coordination/ionic frameworks exhibiting a strong affinity for gaseous molecules as indicated by high binding enthalpies. Other groups have also been interested in lightweight networks and demonstrated the ability of metals ions such as Li^+ to serve as centres within ionic networks.[4–13]

As part of our investigations, an ionic network material of composition Li(inic) (Hinic = isonicotinic acid, 4-pyridinecarboxylic acid, Fig. 1) was reported in 2009.[1] The network possesses parallel channels with a rhombic cross-section that allows the adsorption of a variety of gases. In particular, the Li(inic) network was able to adsorb hydrogen, with a relatively high isosteric enthalpy of adsorption of −9.9 kJ mol^{-1}.[14,15] Attempts to increase the cross-sectional area of the channels and thus improve the storage capacity led to the employment of a longer ligand, the N-oxide form of isonicotinate ($inox^-$, Fig. 1). The structure determination of Li(inox) indicated a tetragonal network that possesses the same topology as PtS with both the Li^+ and $inox^-$ ions serving as 4-connected nodes. Although the topology of Li(inox) is different to that of Li(inic), the network does possess parallel channels, however the adsorption properties proved disappointing as the crystals did not survive the desolvation process.

Although Li(inox) failed to exhibit adsorption behaviour, the network architecture, incorporating relatively large square channels, was particularly appealing. Consequently, other structurally similar components, that might yield analogous networks but prove somewhat more robust, were investigated. Our strategy to create materials that retain their structure upon cycles of adsorption and desorption centred upon enhancement of the lattice energy by using a 2+ metal

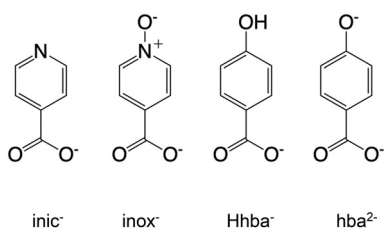

Fig. 1 The bridging anions, $inic^-$, $inox^-$, $Hhba^-$ and hba^{2-}.

[a] *School of Chemistry, University of Melbourne, Victoria 3010, Australia. E-mail: bfa@unimelb.edu.au*
[b] *School of Agriculture, Biomedicine and Environment, La Trobe University, Wodonga, VIC, 3690, Australia*

† Electronic supplementary information (ESI) available: Supplementary figures including TGA traces, powder diffraction patterns and gas adsorption isotherms and information. CCDC 2128440–2128442 and 2128454 for crystallographic data in CIF format. For ESI and crystallographic data in CIF or other electronic format see DOI: 10.1039/d2ce00163b

cation instead of Li^+, and a dianionic ligand in place of $inox^-$. The dianion of 4-hydroxybenzoic acid (hba^{2-}, Fig. 1), which is in fact isoelectronic with $inox^-$, when combined with Zn^{2+} yielded a network of composition, Zn(hba), that was topologically identical to Li(inox) but proved to be far more robust.[15] The reaction of 4-hydroxybenzoic acid with Co(II) yielded a similar structure. Extensive studies of the gas adsorption properties of Zn(hba) were performed, which indicated that the host network was able to reversibly adsorb substantial quantities of a variety of guests without significant deterioration of the host network.[16,17]

Given the successful generation of the porous Zn(hba) networks, we were interested in exploring the types of structures formed when 4-hydroxybenzoic acid is combined with other metal ions under basic conditions. Recently we focussed our attention upon the formation of ionic networks synthesised by the combination of alkali metal hydroxides with H_2hba in aqueous solution. The investigation succeeded in generating a range of new compounds but with dense structures. Except in the case of two Li-hba hydrates, $Li_2(hba)(H_2O)_2$ and $Li_2(hba)(H_2O)_3$, the phenol group remained protonated even under the basic reaction conditions.[18]

We have now extended the scope of our investigation to include further metal-hba systems which we hoped would be porous. Given our long-standing interest in lightweight ionic networks we continued our exploration of Li-based materials and combined 4-hydroxybenzoic acid with Li^+ in nonaqueous solvents. We were hopeful that the absence of water, which readily binds to Li^+ ions, might enhance the prospects of generating an open framework.

Our interest in lightweight ionic networks also prompted the use of Mg^{2+} as the metal centre. Although heavier than Li^+, it is still a relatively lightweight metal and we anticipated that the higher charge on the metal centre may yield a more robust network. Finally, we turned our attention to Cu^{2+}, a dependable and popular choice of metal centre in porous coordination polymers. The rich variety of functional Cu(II) coordination polymers with carboxylate-based ligands provided encouragement that the combination of Cu(II) with 4-hydroxbenzoic acid may yield a stable open network material. We report here the synthesis, structures and properties of three novel coordination polymers of composition $Li_2(hba)(DMF)$ (**1**), $Mg(Hhba)_2(H_2O)_2$·1,4-dioxane (**2**) and $Cu_3(hba)_2(OH)_2(1,4\text{-dioxane})_{1.5}$·0.5(1,4-dioxane) (**3**).

Experimental

Syntheses and general procedures

Commercially available reagents employed in the synthesis of the compounds **1–3** were used without further purification. Microanalyses were performed by either the Microanalytical Unit in the Research School of Chemistry at the Australian National University or the Campbell Microanalytical Laboratory at the University of Otago, NZ. Phase purity was confirmed using X-ray powder diffraction (PXRD) by comparing the bulk product with the calculated powder pattern obtained from the crystal structure determination (ESI†).

$Li_2(hba)(DMF)$ (1). H_2hba (305 mg, 2.21 mmol) and $LiOH·H_2O$ (185 mg, 4.52 mmol) were dissolved in hot MeOH (12 mL). *N*,*N*-Dimethylformamide (DMF) (10 mL) was added to the hot solution. The reaction mixture was stirred on a hotplate set to a temperature of 120 °C. The evaporation of MeOH allowed colourless solid to separate from the hot reaction mixture while being stirred. After an hour of heating, the mixture was allowed to cool slowly to ambient temperature and the solid was filtered off. Inspection of the solid revealed small plate like crystals. Yield: 405 mg (82%). Anal. calcd for Li_2(hba)DMF: C 53.8, N 6.3, H 5.0%. Found: C 53.8, N 6.1, H 5.2%.

$Mg(Hhba)_2(H_2O)_2$·(1,4-dioxane) (2). A suspension of $Mg(OAc)_2·4H_2O$ (1.150 g, 5.36 mmol) and 4-hydroxybenzoic acid (1.148 g, 10.75 mmol) in 30 mL of 1,4-dioxane was allowed to stand for 4 days. Over this period colourless plate-like crystals formed which were filtered, washed (3 × 10 mL 1,4-dioxane) and dried. Upon removal from solution, microanalysis indicates loss of some dioxane and inclusion of some water. Yield: 1.624 g (67%). Anal. calcd for $Mg(Hhba)_2(H_2O)_2$·0.55(1,4-dioxane)·1.25H_2O: C 48.0, H 5.2%. Found: C 48.0, H 5.4%.

$Cu_3(hba)_2(OH)_2(1,4\text{-dioxane})_{1.5}$·0.5(1,4-dioxane) (3). To a solution of $Cu(OAc)_2·H_2O$ (2.500 g, 12.52 mmol) and 4-hydroxybenzoic acid (1.320 g, 9.57 mmol) in 20 mL of ethanol and 110 mL of 1,4-dioxane was added 0.5 mL of 0.01 M NaOH in water. This mixture was then heated at 125 °C in a Teflon-lined autoclave for 2 days. The resulting dark green octahedral-like crystals were filtered, washed (4 × 20 mL 1,4-dioxane) and dried. Upon removal from solution, microanalysis indicates loss of some dioxane and inclusion of some water. Yield: 1.697 g (60%). Anal: calcd for $Cu_3(hba)_2(OH)_2(1,4\text{-dioxane})_{1.5}$·0.75$H_2O$: C 37.4, H 3.7%. Found: C 37.3, H 3.6%.

X-ray crystallography

Single crystal X-ray diffraction measurements on compound **1** were undertaken on an Excalibur, Sapphire 3 Oxford Diffractometer. For compound **2** measurements were performed on an Oxford Diffraction SuperNova diffractometer and for compound **3** data were measured on a Rigaku XtaLAB Synergy-S diffractometer. All data were collected using CuKα radiation (1.54184 Å). In the case of compounds **1** and **2** a crystal was transferred from the mother liquor directly into a protective oil before being mounted on a goniometer where it was placed in a stream of cold nitrogen gas. For compound **3**, crystals were first isolated from the mother liquor before being mounted on a goniometer. For **1**, numerical absorption corrections were carried out using a multifaceted crystal model, and the ABSPACK routine within the CrysAlisPro software package.[19] Empirical absorption corrections were applied for **2** and **3** (ABSPACK within CrysAlisPro).[20] All structures were solved

using SHELXT (intrinsic phasing)[21] and refined using a full-matrix least-squares procedure based on F^2 within the program SHELXL.[22] Crystallographic analyses were conducted within WinGX[23] or OLEX2.[24] Crystallographic data and structural refinement parameters are presented in Table 1. Full details of crystal structure refinements in CIF format are available (ESI†).

The phase change temperature for **3** was determined by measuring cell dimensions using single crystal X-ray diffraction at 20 K intervals between 100 and 250 K. At 220 K the diffraction pattern clearly matched the smaller unit cell whilst at 200 K the diffraction was consistent with the low temperature phase. Measurement at an intermediate temperature of 210 K indicated a cell matching the smaller, high temperature phase but the emergence of additional diffraction spots was also noted. The phase change temperature was determined by both warming and cooling the crystal, indicating the reversibility of the phase transition.

Powder diffraction patterns were measured on an Oxford Diffraction Supernova diffractometer using CuKα radiation or on the powder diffraction beamline at the Australian Synchrotron using radiation of wavelength 0.7745 Å.

Gas adsorption measurements

Volumetric carbon dioxide (CO_2) and methane (CH_4) uptake measurements were performed on a BELSORP HP high pressure gas sorption apparatus. Ultra-high purity (>99.999%) sources of all measurement gases were employed for isotherm analysis. Helium (>99.999% purity) was used as an inert gas. Corrections were applied for non-ideal gas behaviour. Source data for thermophysical properties of CO_2 and CH_4 were obtained from the NIST fluid properties website.[25]

For 273 and 298 K isotherm measurements, sample temperatures were maintained within ±0.1 °C with a Julabo F25-ME heater/chiller unit that circulated fluid through a dual walled steel flask, within a polystyrene box. To allow thermal equilibrium, prior to sorption measurements, the sample was kept at the measurement temperature for a minimum of one hour. Details regarding determination of isosteric CO_2 sorption enthalpies are presented in the ESI.†

Thermogravimetric analysis

Thermogravimetric analysis (TGA) of compound **1** was performed using a METTLER TGA/DSC 1 STAR^e System. TGA analysis for compounds **2** and **3** were conducted using a METTLER TGA/SDTA851 Mettler-Toledo analyzer. Analyses for **1–3** were performed on freshly isolated samples that were held under a stream of N_2 (5 mL min^{-1}) during the experiment. Compound **1** was heated from 40 °C to 450 °C with a temperature increment of 4 °C min^{-1}, while compounds **2** and **3** were heated from 25 °C to 450 °C with a temperature increment of 4 °C min^{-1}.

Results and discussion

Li_2(hba)DMF (1)

The combination of $LiOH{\cdot}H_2O$ and H_2hba in DMF, following the procedure described in the experimental section, yields colourless monoclinic block crystals of Li_2(hba)DMF (**1**). There are four crystallographically distinct Li^+ centres in the asymmetric unit, each of which is in a distorted tetrahedral environment formed by four oxygen atoms. As indicated in Fig. 2a, a carboxylate from one of the hba^{2-} anions links to five Li^+ centres whilst the carboxylate from the second hba^{2-} anion links to four Li^+ centres. Each of the two types of phenolate oxygen atoms serves as a μ_2 bridge between pairs of Li^+ centres. The oxygen atom of one of the crystallographically unique DMF molecules bridges a pair of Li^+ centres whilst the second type binds to a single Li^+ centre.

The structure consists of complex chains, extending in the *c*-direction, in which closely separated Li^+ centres are bridged by oxygen atoms and carboxylate groups. Parallel symmetry-related chains are linked to four neighbouring chains leading to the generation of a 3D network (Fig. 2b). Pairs of neighbouring chains are linked by shoulder-to-shoulder hba^{2-} dianions which form a channel wall as indicated in Fig. 2c. Structures in which Li-carboxylate chains are linked to four parallel chains producing a 3D network are relatively common.[5,12–15,26]

Inspection of Fig. 2b indicates channels with a parallelogram cross-section running in the *c*-direction. The channel dimensions as defined by the separation between the van der Waals surfaces of the channel wall are 4.5 × 6.5 Å but the channels are occupied by coordinated DMF molecules.

$Mg(Hhba)_2(H_2O)_2{\cdot}$(1,4-Dioxane) (2). The room temperature reaction of H_2hba and $Mg(OAc)_2{\cdot}4H_2O$ in 1,4-dioxane yielded colourless rectangular plate-like crystals within four days. Single-crystal X-ray diffraction indicated the compound possesses the formula $Mg(Hhba)_2(H_2O)_2{\cdot}$(1,4-dioxane) (**2**). Each Mg(II) centre is located on a centre of inversion and is coordinated by two *trans* carboxylate oxygen atoms from two $Hhba^-$ anions. *Trans* hydroxyl groups belonging to two other $Hhba^-$ anions and two *trans* water molecules complete an octahedral coordination geometry around the Mg centre (Fig. 3a). Hydrogen bonds extend between each of the hydroxyl groups and the non-coordinated carboxylate oxygen atoms. Whilst the coordination of the phenolic group may be expected to be a rather weak coordinate bond, its participation in a hydrogen bond with the coordinated carboxylate group enhances the interaction between the ligands and the metal.

Each of the four $Hhba^-$ ions links to symmetry related Mg centres within a 2D network possessing the 4,4-topology (Fig. 3b). Within the structure, parallel networks stack on top of each other. Pairs of complementary hydrogen bonds involving a coordinated water molecule and a non-coordinated carboxylate oxygen link the sheets together as

Table 1 Crystallographic data and structure refinement details

	1	**2**	**3**	**4**
Compound	Li_2(hba)(DMF)	Mg(Hhba)$_2$(H_2O)$_2$·(1,4-Dioxane)	Cu_3(hba)$_2$(OH)$_2$(1,4-Dioxane)$_{1.5}$·0.5(1,4-dioxane) 256 K phase	Cu_3(hba)$_2$(OH)$_2$(1,4-Dioxane)$_{1.5}$·0.5(1,4-dioxane) 100 K phase
Formula	$C_{20}H_{22}Li_4N_2O_8$	$C_{18}H_{22}MgO_{10}$	$C_{22}H_{26}Cu_3O_{12}$	$C_{44}H_{52}Cu_6O_{24}$
Formula weight	446.16	422.66	673.08	1346.09
Temperature (K)	130(2)	130(1)	256(1)	100(1)
Wavelength (Å)	1.54184	1.54184	1.54184	1.54184
Crystal system	Monoclinic	Monoclinic	Monoclinic	Monoclinic
Space group	$P2_1/n$	$C2/c$	$P2/n$	$P2/c$
a (Å)	12.2051(3)	10.9854(4)	17.5458(2)	22.4440(2)
b (Å)	15.5772(2)	15.4568(5)	8.30015(10)	8.06390(10)
c (Å)	12.8295(3)	12.8852(5)	18.1756(2)	27.9872(3)
β (°)	116.732(3)	112.395(4)	102.0140(10)	92.3540(10)
Cell volume (Å^3)	2178.46(9)	2022.88(14)	2588.99(5)	5061.02(9)
Z	4	4	4	4
Density (calculated) (mg m^{-3})	1.360	1.388	1.727	1.767
Absorption coefficient (mm^{-1})	0.847	1.242	3.407	3.486
F(000)	928	888	1364	2728
Crystal size (mm)	0.31 × 0.10 × 0.08	0.06 × 0.10 × 0.15	0.29 × 0.26 × 0.25	0.29 × 0.27 × 0.23
θ range for data collection (°)	4.15 to 76.88	5.35 to 74.383	3.185 to 76.490	3.161 to 76.533
Reflections collected	10 779	3882	18 538	37 599
Independent reflections	4548 [R_{int} = 0.0182]	2008 [R_{int} = 0.0259]	5243 [R_{int} = 0.0249]	10 168 [R_{int} = 0.0298]
Completeness	98.9% (to θ = 76.88°)	99.8% (to θ = 74.383°)	99.9% (to θ = 76.490°)	99.7% (to θ = 76.533°)
Goodness-of-fit on F^2	1.050	1.056	1.069	1.062
Final R indices [$I > 2\sigma(I)$]	R_1 = 0.0406, wR_2 = 0.1119	R_1 = 0.0400, wR_2 = 0.1046	R_1 = 0.0432, wR_2 = 0.1191	R_1 = 0.0394, wR_2 = 0.1135
R indices (all data)	R_1 = 0.0498, wR_2 = 0.1164	R_1 = 0.0497, wR_2 = 0.1118	R_1 = 0.0468, wR_2 = 0.1219	R_1 = 0.0419, wR_2 = 0.1156
Largest diff. peak and hole (e Å^{-3})	0.52 and −0.24	0.36 and −0.29	1.07 and −0.70	1.00 and −0.74

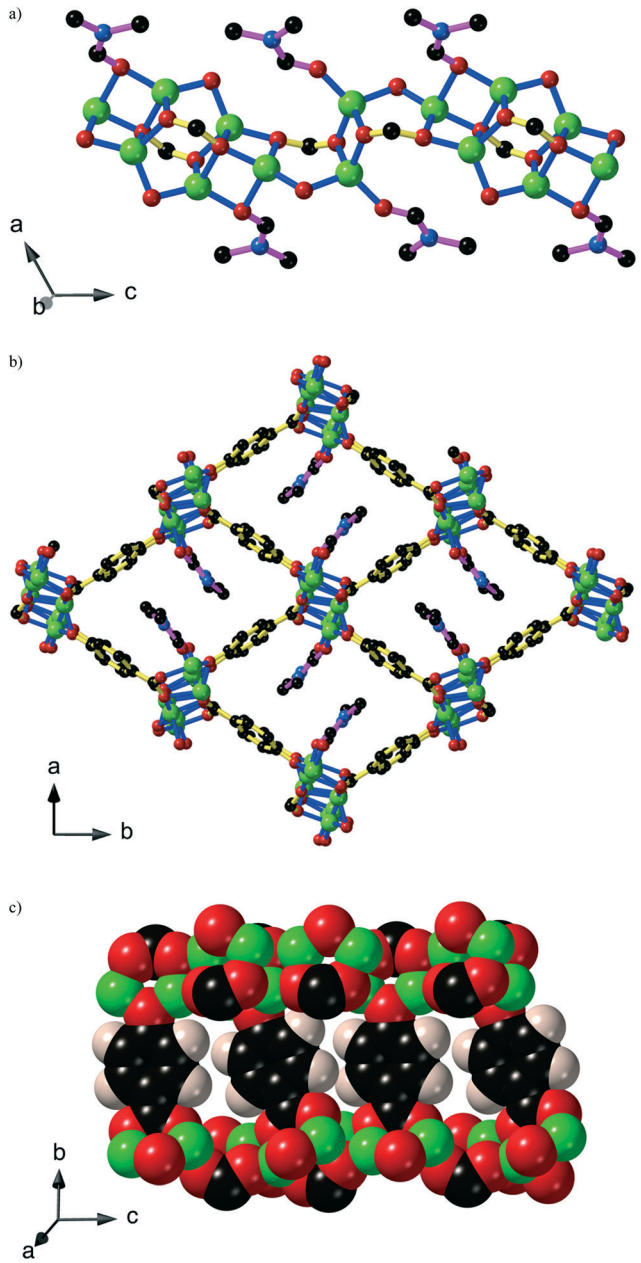

Fig. 2 The structure of **1** showing a) a Li–O chain extending in the *c*-direction, b) the 3D structure and c) a space-filling representation of a pair of chains linked by the hba^{2-} anions to form a channel wall. Colour code: O red, N blue, C black, Li green and H light brown. H atoms have been omitted from (a) and (b) for clarity.

indicated in Fig. 3c. As a consequence of the hydrogen bonding, the parallel sheets are offset from each other resulting in the formation of channels, the direction of which is parallel with the *c*-axis and is inclined by an angle of ~40° to the normal of the 4,4 network. As indicated in Fig. 3c, the second hydrogen atom of the coordinated water molecule participates in a hydrogen bond with a 1,4-dioxane molecule which in turn forms a second hydrogen bond to a coordinated water molecule belonging to an adjacent sheet. Fig. 3d shows the rhombic shaped channels which extend in

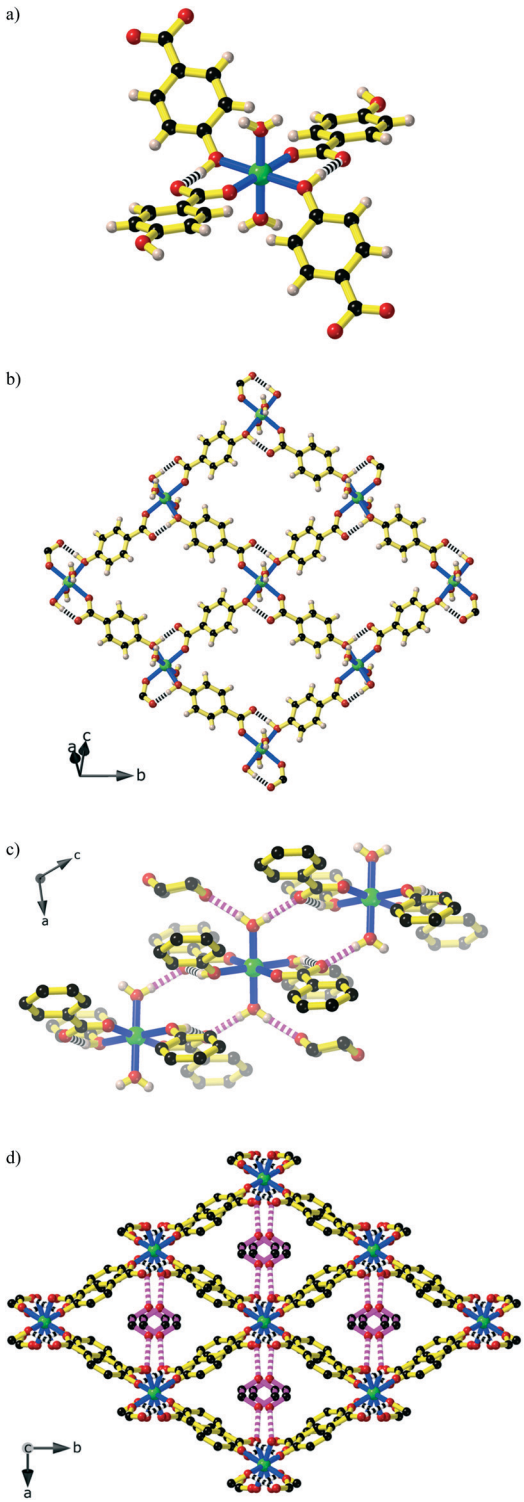

Fig. 3 The structure of $Mg(Hhba)_2(H_2O)_2 \cdot$(1,4-dioxane) showing a) the coordination environment of the Mg centre, b) the $Mg(Hhba)_2(H_2O)_2$ network with Mg centres linked by $Hhba^-$ ligands, c) the complementary hydrogen bonding between three parallel sheets and d) a view along the *c*-direction highlighting the channels formed by the offset stacking of the 4,4-networks. Colour code: Mg green, O red, C black and H light brown; black and white striped connections indicate hydrogen bonds between the carboxylate group of one $Hhba^-$ anion and a hydroxyl group of a second $Hhba^-$ anion; pink and white striped connections indicate intersheet hydrogen bonds. Selected hydrogen atoms have been omitted for clarity.

the *c*-direction and are filled with the hydrogen bonded 1,4-dioxane molecules. If the 1,4-dioxane molecules are ignored, the void space is estimated to be 31% of the crystal volume as calculated by Mercury (1.2 Å probe radius).[27]

$Cu_3(hba)_2(OH)_2(1,4\text{-Dioxane})_{1.5}\cdot 0.5(1,4\text{-dioxane})$ (3)

The reaction of $Cu(OAc)_2\cdot H_2O$, H_2hba and a small volume of dilute aqueous NaOH in 1,4-dioxane at 125 °C yields dark green octahedral-shaped crystals of composition $Cu_3(hba)_2(OH)_2(1,4\text{-dioxane})_{1.5}\cdot 0.5(1,4\text{-dioxane})$ (**3**). The structure of **3** recorded at a temperature of 256 K consists of a single 3D network in which Cu(II) centres are linked by hba^{2-} dianions, hydroxide ions and 1,4-dioxane molecules. There are three crystallographically distinct Cu centres (Cu1, Cu2 and Cu3) in the structure that form chains (Fig. 4a). Pairs of Cu1 centres are linked by two phenolate oxygen atoms within 4-membered rings; pairs of Cu3 centres are similarly linked to form 4-membered rings. Cu2 and Cu1 centres as well as Cu2 and Cu3 centres are each linked by μ_2-hydroxide anions and O–C–O carboxylate units to form 6-membered rings. Thus, the chain consists of corner shared 4-membered and 6-membered rings in a 6,6,4,6,6,4 sequence along the length of the chain as depicted in Fig. 4a. The rings within the chain are approximately co-planar and the Cu–O bonds that form the rings are all less than 2.0 Å. In addition to the atoms of the anionic groups bound to each of the Cu centres, an oxygen atom of a 1,4-dioxane molecule occupies an apical position of a square pyramidal coordination geometry on the Cu2 and Cu3 centres. On Cu1 centres, an oxygen atom of a 1,4-dioxane molecule occupies the apical site ~62% of the time according to the refinement of site occupancies. The orientation of the apical Cu–O (1,4-dioxane) bond alternates along the length of the chain and represents a relatively weak coordinate interaction with the Cu(II) centres with bond distances in the range 2.330(3)–2.684(5) Å. The coordinated 1,4-dioxane molecules form bridges between parallel chains resulting in the generation of a sheet that lies in the *a*–*b* plane as depicted in Fig. 4b. Within this sheet, Cu3 centres from one chain are linked to Cu3 centres from neighbouring parallel chains. Although Cu2 is always coordinated by a 1,4-dioxane molecule, the 1,4-dioxane is disordered over two sites, one of which has 62% site occupancy, whilst the second orientation does not form an interchain bridge. The dominant orientation of the 1,4-dioxane molecule results in a bridge between the Cu2 centres on one chain and the Cu1 centres on neighbouring chains.

Inspection of Fig. 4b reveals hba^{2-} dianions extending almost normal to the parallel sheets and forming bridges to chains in neighbouring sheets. Although the adjacent sheets are symmetry related to the sheet depicted in Fig. 4b, the Cu chains in the adjacent sheets run in the [−1 1 0] direction in contrast to the [1 1 0] direction indicated in Fig. 4b. As a consequence, each Cu-chain running in the [1 1 0] direction links to an infinite number of symmetry related chains

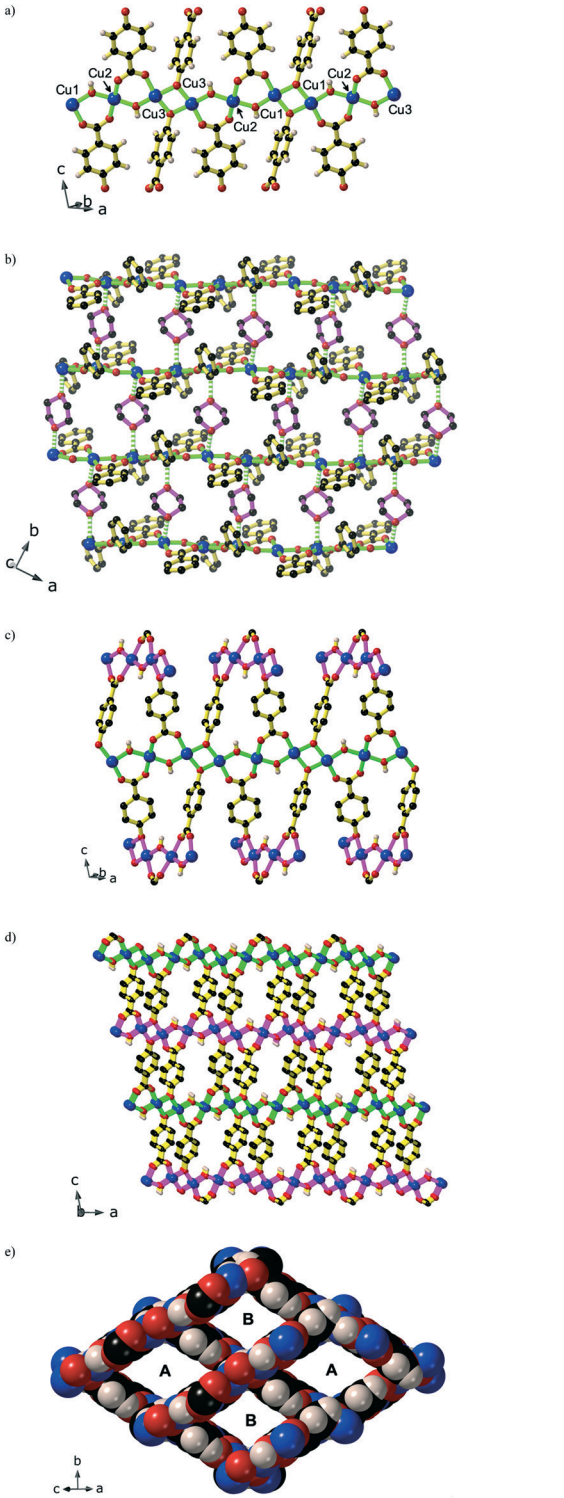

Fig. 4 The structure of **3** showing a) a single '6,6,4,6,6,4' chain in which Cu1, Cu2 and Cu3 centres are linked by carboxylate, phenolate and hydroxo groups, b) '6,6,4,6,6,4' chains linking to symmetry-related chains through bridging 1,4-dioxane molecules to form a 2D network in the *a*–*b* plane; H atoms omitted, c) a single chain linking to six symmetry-related chains in neighbouring sheets through pairs of hba^{2-} anions; hba^{2-} H atoms omitted d) the 3D structure (with 1,4-dioxane molecules omitted); hba^{2-} H atoms omitted and e) a space-filling representation of the 3D structure indicating rhombic-shaped channels running in the [1 0 1] direction. Colour code: Cu blue; O red, C black, and H light brown.

running in the [−1 1 0] direction. A section of a chain extending in the [1 1 0] direction forming links to six neighbouring chains running in the [−1 1 0] direction is presented in Fig. 4c, which also indicates that a single chain is linked to another chain by a pair of hba^{2-} dianions. These two hba^{2-} anions are separated by a Cu–μ_2OH–Cu link within a single chain. The cross-linking of the chains results in the formation of a 3D network (Fig. 4d). Within Fig. 4d the chains in the green layer extend in the [1 1 0] direction whilst those in the pink layer extend in the [−1 1 0] direction.

When the 3D structure is viewed down the [1 0 1] direction, channels with a rhombic cross-section are apparent. There are two crystallographically distinct types of channels labelled A and B in Fig. 4e. The internal dimensions of channel A are 4.5 × 4.5 Å as defined by the separation of van der Waals surfaces, whereas channel B is a little smaller, 4.0 × 4.0 Å. Channel A is occupied by non-coordinating 1,4-dioxane molecules in addition to 1,4-dioxane molecules bridging Cu3 centres. In contrast to the ordered 1,4-dioxane molecules in channel A, channel B is filled with disordered 1,4-dioxane, bound to Cu2 centres.

Diffraction data collected at a temperature of 100 K indicated a phase change occurs upon slow cooling of the crystal (see **4** in Table 1). The unit cell obtained at 100 K indicates a re-orientation of the crystallographic axes in the *a*–*c* plane with the new axes corresponding to face diagonals of the original cell. The space group of the 100 K structure is *P*2/*c*. The 100 K structure is similar to the 256 K structure, but the asymmetric unit is twice as large. The main difference relates to the interaction of 1,4-dioxanes with the Cu(II) centres. It is interesting to compare the 1,4-dioxane in the 256 K structure, which bridges Cu3 centres, with the corresponding Cu centres in the 100 K structure as indicated in Fig. 5. At 256 K the Cu3 centres, which are 7.3842(9) Å apart, are linked by 1,4-dioxane in a chair conformation, that binds through its 'equatorial' sites. At 100 K the corresponding Cu centres are Cu3 and Cu6. The Cu6 centres are 7.4110(7) Å apart and are coordinated by O atoms binding through equatorial sites. The Cu3 centres at 100 K are now 6.6823(8) Å apart and are coordinated by O atoms binding through axial sites. A general shortening of the Cu–O(1,4-dioxane) bonds is also apparent with bond distances in the range 2.330(3)–2.684(5) Å at 256 K compared to 2.303(2)–2.551(2) Å at 100 K.

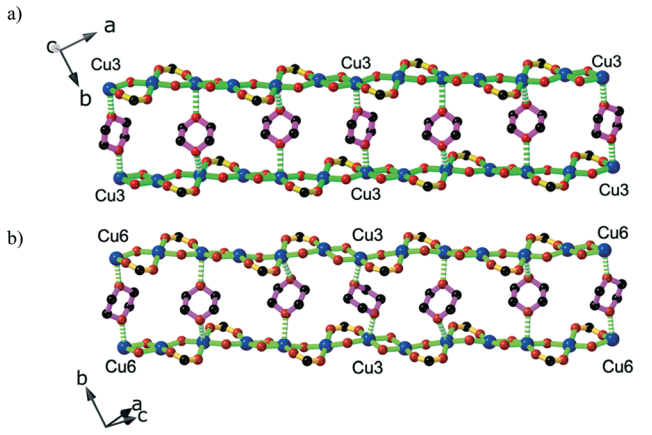

Fig. 5 The structure of **3** showing the 1,4-dioxane links between Cu(II) within parallel chains at a) 256 K and b) 100 K.

Measurement of cell dimensions within the 100–256 K range, using single crystal X-ray diffraction, reveal that a reversible transition between the phases occurs between 200 and 220 K with retention of single crystal character.

The structure of **3** shares some similarities with the MIL-53 family of MOF structures in which parallel chains containing metal centres are linked by μ_2-hydroxido ions and carboxylate groups.[28] Each chain links to four other chains through the bridging ligand to create a structure with large parallel channels. In the case of **3**, the chains, as depicted in Fig. 4a, link to an infinite number of other chains through bridging hba^{2-} ligands. Links to a further two parallel chains occur through 1,4-dioxane bridges.

Discussion of structures

Within the three different compounds there is considerable variation in the connectivities of the structures, yet despite these differences there are some remarkable similarities. In all three structures the phenol (in the case of $Hhba^-$) or the phenolate O atom (in the case of hba^{2-}) links metal centres at one end whilst the carboxylate group links to one or more metal centres at the other end of the ligand. Furthermore, in all structures parallel rhombic-shaped (or close to rhombic-shaped) channels are apparent and occupied by solvent molecules. Similarities with respect to the generation of crystalline networks possessing parallel 4-sided channels extend to the previously reported Zn(hba) and Co(hba) structures.[15] Within Zn(hba) and Co(hba), square channels arise from the bridging of chains of metal centres, linked by carboxylate and phenolate groups to symmetry-related chains. Further similarities are apparent with Li(inox) (inox = the N-oxide of isonicotinate)[15] which has the same topology as Zn(hba) and Co(hba); the $inox^-$ anion is structurally similar to hba^{2-} in addition to being isoelectronic. In contrast to Zn(hba), Co(hba) and Li(inox), compounds **1**–**3** each have solvent molecules either directly bound to metal centres or alternatively forming hydrogen bonds with coordinated water molecules. These solvent molecules appear to play a key structural role.

Thermogravimetric analyses

Thermogravimetric analysis (TGA) of **1** (Fig. S1†) shows a small gradual decrease in mass followed by a significant mass loss beyond 225 °C. Presumably the isolated solid, Li_2(hba)(DMF), adsorbs water from the atmosphere leading to a larger than expected mass loss for the initial desolvation process. The total mass loss up to 340 °C is ~43% which is consistent with the loss of DMF and water from a material of composition, Li_2(hba)(DMF)·2H_2O (42%). A shoulder is apparent in this section of the trace which may signify the loss of a structurally different DMF molecule. The TGA trace

begins to plateau about 330 °C before a further decrease begins at ~370 °C, which presumably is associated with decomposition of the hba^{2-} ligands. For compound **2** (Fig. S2†) a mass loss begins near 125 °C and is completed by ~225 °C. This decrease in mass of approximately 31% would appear to be associated with the loss of both 1,4-dioxane and the coordinated water molecules (calcd 29.4%). A shoulder in the trace during the mass loss between 125 and 225 °C is suggestive of at least two different mass loss processes. Beyond 225 °C a second mass loss process of a similar magnitude (~29%) is underway which seems likely to correspond to the loss of H_2hba (calcd 32.4%), leaving a material of composition Mg(hba) behind. TGA on **3** (Fig. S3†) indicates a mass loss of ~22% which begins at ~60 °C and is completed by 150 °C. This agrees closely with the expected mass loss of 1,4-dioxane and water of 22.7% from $Cu_3(hba)_2(OH)_2(1,4\text{-dioxane})_{1.5}\cdot 0.75H_2O$ (see microanalytical results). The TGA indicates a plateau following this mass loss before another mass loss at 260 °C.

Gas adsorption studies

Our earlier experiments involving Zn^{2+} and Co^{2+} coordination polymers of hba^{2-} revealed their open frameworks are stable to solvent loss and adsorb appreciable quantities of gas and the vapours of some volatile substances.[15,16] Representations of the void boundaries in **1**, **2** and **3**, presented in Fig. 6, provided encouragement that upon loss of solvent from channels that the compounds will display adsorption. The calculated void volume of compounds **1**–**3**, based on the removal of all coordinated and uncoordinated solvent (DMF, 1,4-dioxane and H_2O) is 40, 37 and 49% respectively of the crystal volume. In contrast to the Zn^{2+} and Co^{2+} coordination polymers of hba^{2-}, the intra-network spaces of **1**–**3** are occupied, at least in part, by solvent that is bound to the network metal centres, DMF in the case of **1**, water in **2** and 1,4-dioxane in **3**. The presence of coordinated solvent in network channels may be considered desirable in a host material, as it offers the prospect of the generation of channels containing open metal sites upon the removal of the solvent. In host materials, exposed surfaces of metal ions are known to act as favourable guest-binding sites.[29]

For gas sorption experiments on **1**–**3**, thermogravimetric investigations (Fig. S1–S3, ESI†) provided guidance as to the conditions required to remove coordinated solvent from each compound. Further experimental information regarding gas sorption and structural studies on heated samples of **1**–**3** are presented in the ESI.†

A carbon dioxide (CO_2) isotherm performed on **1** and measured at 298 K indicated negligible uptake (Fig. S8†). The result contrasts with work reported by Feng, Bu and coworkers who have shown that activated $Li_2(hba)(MeOH)_2$ yields a material capable of adsorbing H_2 and CO_2.[11] Isotherm measurements (Fig. 7a) conducted on **2** indicate some uptake of CO_2. At atmospheric pressure, an uptake of 8 mg and 5 mg of CO_2 g^{-1} of solid was recorded at 273 and 298 K, respectively. At ~1200 kPa, 33 mg of CO_2 g^{-1} (273 K) and 19 mg CO_2 g^{-1} (298 K) was adsorbed. In contrast, a 273 K methane isotherm (Fig. 7a) shows almost no uptake of the gas up to 1200 kPa. CO_2 adsorption isotherms recorded at 298 and 273 K on **3** (Fig. 7b) reveal a relatively modest uptake of gas at atmospheric pressure. At 1200 kPa, 11 mg (298 K) and 25 mg (273 K) of CO_2 g^{-1} are adsorbed. Similar to compound **2**, a 273 K CH_4 isotherm measurement on **3** (Fig. 7b) indicates very limited uptake of the gas up to a pressure of 1140 kPa. Examples of porous materials showing superior CO_2 uptake over CH_4 are reasonably common.[30] In many of these cases, workers have attributed the preferred CO_2 over CH_4 uptake to size exclusion mechanisms,[31] greater polarizability of CO_2 compared to CH_4 and preferred binding of CO_2 to pore surfaces[32,33] in addition to superior CO_2 adsorption kinetics.[34]

For all three compounds (**1**–**3**), the limited CO_2 and CH_4 uptakes suggest the as-synthesised metal–4-hydroxybenzoate anion networks are not retained upon the removal of solvent. Heating compound **1** under vacuum during the activation

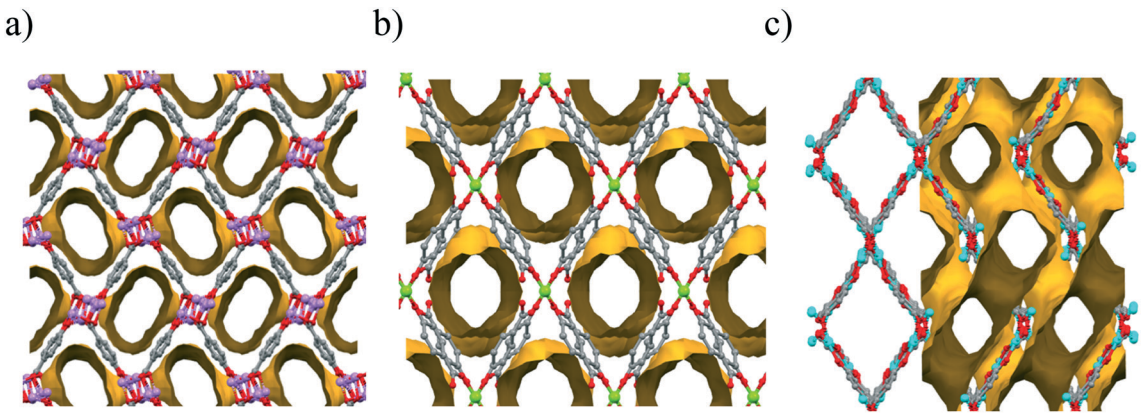

Fig. 6 Representations of potential framework voids occupied by coordinated and uncoordinated solvent molecules in a) **1** (viewed along the [0 0 1] direction), b) **2** (viewed along the [0 0 1] direction) and c) **3** (viewed along the [1 0 1] direction); in **3** the channel boundary surfaces obscure the underlying framework which is represented on the left-hand side.

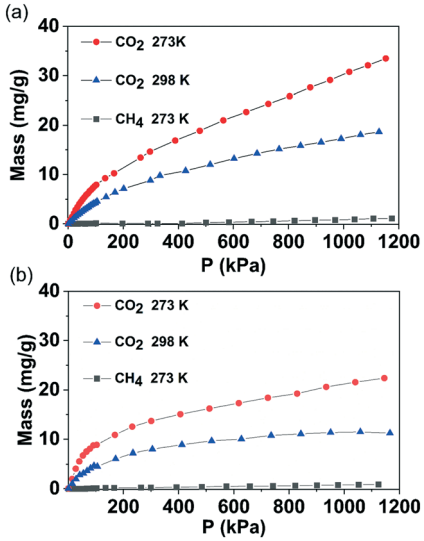

Fig. 7 CO_2 (298 and 273 K) and CH_4 (273 K) sorption isotherms for a) **2** and b) **3**.

process leads to the loss of DMF and presumably the reorganisation of the remaining components within **1** to yield a denser structure. Powder X-ray diffraction analysis of the solid indicates a crystalline material with a powder diffraction pattern that matches the calculated pattern of $Li_2(hba)(H_2O)_3$ (Fig. S5†).[18] It would appear that the $Li_2(hba)$ residue is hygroscopic and has adsorbed water from the atmosphere upon its removal from the gas adsorption instrument.

Compound **2** differs from **1** and **3** in that it contains both coordinated H_2O, and non-coordinated solvent, 1,4-dioxane. While **2** shows some CO_2 uptake, powder diffraction (Fig. S6†) indicates the compound becomes a largely amorphous residue upon heating. Synchrotron PXRD studies of **3** (Fig. S7†) show the removal of 1,4-dioxane also leads to structural rearrangements. The presence of both sharp and broad peaks in the pattern of the solvent-free **3** suggest multiple phases exist in the desolvated residue. The addition of the original solvents to desolvated samples of **2** and **3** failed to restore the crystallinity of the solids.

The CO_2 adsorption by **2** and **3** at two different temperatures allows estimation of the isosteric CO_2 sorption enthalpies for these compounds. The interaction of molecules such as CO_2 with exposed metal centres in networks, is expected to result in elevated binding enthalpies (typically with magnitudes greater than 30 kJ mol^{-1}) and thus, such calculations can provide an indication of the presence or accessibility of coordinatively unsaturated metal centres.[29] Isosteric binding enthalpies for CO_2 by **2** and **3** were calculated using the virial method (ESI†).[35,36] For **2** and **3** the calculations indicate that during the early CO_2 loading phase the binding enthalpies are −22 kJ mol^{-1} and −21 kJ mol^{-1} respectively. These modest CO_2 binding enthalpies suggest the absence/inaccessibility of metal coordination sites for the desolvated residues of **2** and **3**.

Concluding remarks

The three compounds (**1**–**3**) described in this report are all examples of network materials in which metal centres are linked by anions of 4-hydroxybenzoic acid. As with the previously reported structures, Zn(hba) and Co(hba), solvent filled channels are generated, but unlike Zn(hba) and Co(hba), solvent molecules are coordinated to the metal centres. The topologies of the Li, Mg and Cu structures are all very different yet each of the structures possesses parallel channels that have close to rhombic cross-sections as depicted in Fig. 6. This structural similarity extends to Zn(hba) and Co(hba) where parallel channels have a square cross-section.

Although Zn(hba) has shown itself to be an excellent adsorbent material for a wide range of guests, including gas molecules and inhalation anaesthetics, the relatively poor adsorption displayed by **1**–**3** is presumably due to the collapse of the crystal structure upon removal of the coordinated solvent. This structural deterioration is perhaps not surprising in the case of compounds **1** and **2**, since the removal of the solvent from the coordination sphere of the metal centre would result in a significant proportion of the metal ion's surface, Li^+ in **1** and Mg^{2+} in **2**, being left exposed. The transformation to coordinatively saturated metal centres would seem to rely upon a reorganisation of the network components to produce a denser structure that presumably exhibits limited adsorptive behaviour.

In compound **3** almost all Cu(II) centres are 5-coordinate with a square pyramidal environment. The apical position is occupied by a coordinated 1,4-dioxane molecule. Given the ability of Cu(II) centres to adopt square planar coordination, it would seem plausible for the removal of the solvent to proceed with retention of the framework arrangement, yielding a structure in which vacant coordination sites on the Cu(II) may provide a 'docking' location for guest molecules. Perhaps one reason why removal of the 1,4-dioxane does not result in a stable structure relates to the key structural role of the bridging solvent molecule. As depicted in Fig. 4b the parallel chains are bridged by the 1,4-dioxane molecules to form sheets. Removal of the 1,4-dioxane molecules, which act as 'braces' between the parallel chains, would seem likely to result in a loss of structural integrity.

Although this current work has not succeeded in yielding highly adsorbing Li, Mg or Cu-based structures, the use of alternative solvents that may not bind as strongly to metal centres but can assist in templating channels in the crystal growth process, may yield materials with useful adsorbent properties. Work is continuing in the investigation of these systems.

Conflicts of interest

There are no conflicts of interest to declare.

Acknowledgements

The authors gratefully the financial support of the Australian Research Council (DP0663872). Part of this work was undertaken on the Powder Diffraction Beamline at the Australian Synchrotron (part of ANSTO).

References

1 K. M. Fromm, *Coord. Chem. Rev.*, 2008, **252**, 856–885.
2 D. Banerjee and J. B. Parise, *Cryst. Growth Des.*, 2011, **11**, 4704–4720.
3 M. A. Alnaqbi, A. Alzamly, S. H. Ahmed, M. Bakiro, J. Kegere and H. L. Nguyen, *J. Mater. Chem. A*, 2021, **9**, 3828–3854.
4 D. Banerjee, L. A. Borkowski, S. J. Kim and J. B. Parise, *Cryst. Growth Des.*, 2009, **9**, 4922–4926.
5 D. Banerjee, S. J. Kim, W. Li, H. Wu, J. Li, L. A. Borkowski, B. L. Philips and J. B. Parise, *Cryst. Growth Des.*, 2010, **10**, 2801–2805.
6 R. El Osta, M. Frigoli, J. Marrot, M. E. Medina, R. I. Walton and F. Millange, *Cryst. Growth Des.*, 2012, **12**, 1531–1537.
7 S. B. Aliev, D. G. Samsonenko, M. I. Rakhmanova, D. N. Dybtsev and V. P. Fedin, *Cryst. Growth Des.*, 2014, **14**, 4355–4363.
8 A. Clough, S.-T. Zheng, X. Zhao, Q. Lin, P. Feng and X. Bu, *Cryst. Growth Des.*, 2014, **14**, 897–900.
9 T. Koltunova, D. Samsonenko, D. Dybtsev and V. Fedin, *J. Struct. Chem.*, 2017, **58**, 1048–1055.
10 D. Pugh, E. Ashworth, K. Robertson, L. C. Delmas, A. J. White, P. N. Horton, G. J. Tizzard, S. J. Coles, P. D. Lickiss and R. P. Davies, *Cryst. Growth Des.*, 2018, **19**, 487–497.
11 X. Zhao, M. S. Shimazu, X. Chen, X. Bu and P. Feng, *Angew. Chem., Int. Ed.*, 2018, **57**, 6208–6211.
12 R. El Osto, M. Frigoli, J. Marrot, N. Guillou, H. Chevreau, R. I. Walton and F. Millange, *Chem. Commun.*, 2012, **48**, 10639–10641.
13 J. C. Houlihan, S. C. Moratti and L. R. Hanton, *Dalton Trans.*, 2020, **49**, 12009–12017.
14 B. F. Abrahams, M. J. Grannas, T. A. Hudson and R. Robson, *Angew. Chem., Int. Ed.*, 2010, **49**, 1087–1089.
15 B. F. Abrahams, A. D. Dharma, M. J. Grannas, T. A. Hudson, H. E. Maynard-Casely, G. R. Oliver, R. Robson and K. F. White, *Inorg. Chem.*, 2014, **53**, 4956–4969.
16 K. F. White, B. F. Abrahams, R. Babarao, A. D. Dharma, T. A. Hudson, H. E. Maynard-Casely and R. Robson, *Chem. – Eur. J.*, 2015, **21**, 18057–18061.
17 B. F. Abrahams, A. D. Dharma, P. S. Donnelly, T. A. Hudson, C. J. Kepert, R. Robson, P. D. Southon and K. F. White, *Chem. – Eur. J.*, 2017, **23**, 7871–7875.
18 B. F. Abrahams, C. J. Commons, T. A. Hudson, R. Sanchez Arlt, K. F. White, M. Chang, J. J. Jackowski, M. Lee, S. X. Lee, H. D. Liu, B. M. Mei, J. E. Meng, L. Poon, X. Xu and Z. Yu, *Acta Crystallogr., Sect. C: Struct. Chem.*, 2021, **77**, 340–353.
19 *CrysAlisPRO*, Oxford Diffraction/Agilent Technologies UK Ltd, Yarnton, England, 2015.
20 *CrysAlisPRO*, Oxford Diffraction/Agilent Technologies UK Ltd, Yarnton, England, 2018.
21 G. Sheldrick, *Acta Crystallogr., Sect. A: Found. Adv.*, 2015, **71**, 3–8.
22 G. Sheldrick, *Acta Crystallogr., Sect. C: Struct. Chem.*, 2015, **71**, 3–8.
23 L. Farrugia, *J. Appl. Crystallogr.*, 2012, **45**, 849–854.
24 O. V. Dolomanov, L. J. Bourhis, R. J. Gildea, J. A. K. Howard and H. Puschmann, *J. Appl. Crystallogr.*, 2009, **42**, 339–341.
25 https://webbook.nist.gov/chemistry/fluid/.
26 K. F. White, B. F. Abrahams, H. Maynard-Casely and R. Robson, *Cryst. Growth Des.*, 2014, **14**, 4602–4609.
27 C. F. Macrae, I. Sovago, S. J. Cottrell, P. T. A. Galek, P. McCabe, E. Pidcock, M. Platings, G. P. Shields, J. S. Stevens, M. Towler and P. A. Wood, *J. Appl. Crystallogr.*, 2020, **53**, 226–235.
28 F. Millange, C. Serre and G. Férey, *Chem. Commun.*, 2002, 822–823.
29 Ü. Kökçam-Demir, A. Goldman, L. Esrafili, M. Gharib, A. Morsali, O. Weingart and C. Janiak, *Chem. Soc. Rev.*, 2020, **49**, 2751–2798.
30 H. Li, L. Li, R.-B. Lin, W. Zhou, Z. Zhang, S. Xiang and B. Chen, *EnergyChem*, 2019, **1**, 100006.
31 W. Zhuang, D. Yuan, D. Liu, C. Zhong, J.-R. Li and H.-C. Zhou, *Chem. Mater.*, 2012, **24**, 18–25.
32 D. Britt, H. Furukawa, B. Wang, T. G. Glover and O. M. Yaghi, *Proc. Natl. Acad. Sci. U. S. A.*, 2009, **106**, 20637–20640.
33 S.-J. Bao, R. Krishna, Y.-B. He, J.-S. Qin, Z.-M. Su, S.-L. Li, W. Xie, D.-Y. Du, W.-W. He and S.-R. Zhang, *J. Mater. Chem. A*, 2015, **3**, 7361–7367.
34 P. Nugent, Y. Belmabkhout, S. D. Burd, A. J. Cairns, R. Luebke, K. Forrest, T. Pham, S. Ma, B. Space and L. Wojtas, *Nature*, 2013, **495**, 80–84.
35 L. Czepirski and J. JagieŁŁo, *Chem. Eng. Sci.*, 1989, **44**, 797–801.
36 A. Nuhnen and C. Janiak, *Dalton Trans.*, 2020, **49**, 10295–10307.